JACS
JOURNAL OF THE AMERICAN CHEMICAL SOCIETY

Article

pubs.acs.org/JACS

Reactivity and O_2 Formation by Mn(IV)- and Mn(V)-Hydroxo Species Stabilized within a Polyfluoroxometalate Framework

Roy E. Schreiber,[†] Hagai Cohen,[‡] Gregory Leitus,[‡] Sharon G. Wolf,[‡] Ang Zhou,[§] Lawrence Que, Jr.,[§] and Ronny Neumann*[,†]

[†]Department of Organic Chemistry, Weizmann Institute of Science, Rehovot 76100, Israel

[‡]Department for Chemical Research Support, Weizmann Institute of Science, Rehovot 76100, Israel

[§]Department of Chemistry and Center for Metals in Biocatalysis, University of Minnesota, Minneapolis, Minnesota 55455, United States

Supporting Information

ABSTRACT: Manganese(IV,V)-hydroxo and oxo complexes are often implicated in both catalytic oxygenation and water oxidation reactions. Much of the research in this area is designed to structurally and/or functionally mimic enzymes. On the other hand, the tendency of such mimics to decompose under strong oxidizing conditions makes the use of molecular inorganic oxide clusters an enticing alternative for practical applications. In this context it is important to understand the reactivity of conceivable reactive intermediates in such an oxide-based chemical environment. Herein, a polyfluoroxometalate (PFOM) monosubstituted with manganese, $[NaH_2(Mn\text{-}L)W_{17}F_6O_{55}]^{q-}$, has allowed the isolation of a series of compounds, Mn(II, III, IV and V), within the PFOM framework. Magnetic susceptibility measurements show that all the compounds are high spin. XPS and XANES measurements confirmed the assigned oxidation states. EXAFS measurements indicate that Mn(II)PFOM and Mn(III)PFOM have terminal aqua ligands and Mn(V)PFOM has a terminal hydroxo ligand. The data are more ambiguous for Mn(IV)PFOM where both terminal aqua and hydroxo ligands can be rationalized, but the reactivity observed more likely supports a formulation of Mn(IV)PFOM as having a terminal hydroxo ligand. Reactivity studies in water showed unexpectedly that both Mn(IV)-OH-PFOM and Mn(V)-OH-PFOM are very poor oxygen-atom donors; however, both are highly reactive in electron transfer oxidations such as the oxidation of 3-mercaptopropionic acid to the corresponding disulfide. The Mn(IV)-OH-PFOM compound reacted in water to form O_2, while Mn(V)-OH-PFOM was surprisingly indefinitely stable. It was observed that addition of alkali cations (K^+, Rb^+, and Cs^+) led to the aggregation of Mn(IV)-OH-PFOM as analyzed by electron microscopy and DOSY NMR, while addition of Li^+ and Na^+ did not lead to aggregates. Aggregation leads to a lowering of the entropic barrier of the reaction without changing the free energy barrier. The observation that O_2 formation is fastest in the presence of Cs^+ and ~fourth order in Mn(IV)-OH-PFOM supports a notion of a tetramolecular Mn(IV)-hydroxo intermediate that is viable for O_2 formation in an oxide-based chemical environment. A bimolecular reaction mechanism involving a Mn(IV)-hydroxo based intermediate appears to be slower for O_2 formation.

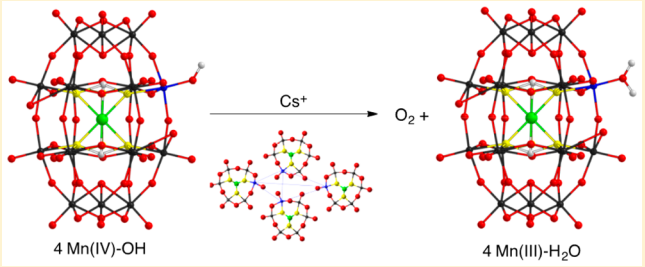

INTRODUCTION

Manganese-based catalysts are of interest in various reactions involving low valent species, for example, as mimics of superoxide dismustase and hydrogen peroxide catalases that decompose $O_2^{\bullet-}$ and H_2O_2.[1,2] On the other hand higher valent species are important in the context of water oxidation[3] and oxygenation reactions.[4] A key issue in this later field has been the isolation and identification of high valent manganese species, such as Mn(V)-oxo, Mn(IV)-oxo and Mn(IV)-hydroxo species, designed to lead to understanding of manganese-based oxygenations and water oxidation, that is, O_2 evolving reactions. Such investigations have been carried out using various coordination platforms such as porphyrins,[5] corroles,[6] corrolozines,[7] and others.[8] For the development of practical catalysts it is important to develop and study compounds that will be stable in highly oxidizing environments. Polyoxometalates, typically anionic oxide clusters of molybdenum and tungsten, are a class of compounds that are indeed stable to even very strongly oxidizing environments such as ozone that also can be soluble in water. Importantly, insertion of a transition metal into the polyoxometalate to form so-called transition metal-substituted polyoxometalates can lead to a formulation where a transition metal is ligated by a polyoxometalate. First row transition metal (Co, Mn) containing polyoxometalates have been reported as water oxidation catalysts,[9] and Mn containing polyoxometalates have been used in various oxygenation reactions.[10] Such polyox-

Received: April 2, 2015
Published: June 12, 2015

DOI: 10.1021/jacs.5b03456
J. Am. Chem. Soc. 2015, 137, 8738−8748

ometalates acting as ligands have also been shown to have a good potential to stabilize high oxidation state species. In this area a Mn(V)-oxo species was identified as an effective oxygen donor in an organic solvent,[11] and a dimeric Co(III)-oxyl species was efficient for O_2 formation and C−H bond activation in water.[12] Transition metal substituted polyfluoroxometalates of the quasi Wells−Dawson structure, Figure 1, are

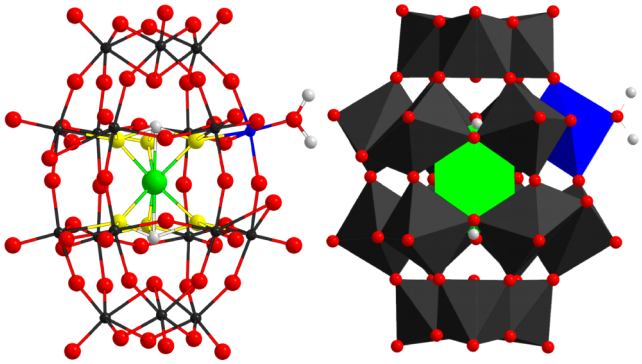

Figure 1. Ball and stick (left) and polyhedral (right) representation of a $[NaH_2(TM\text{-}H_2O)W_{17}F_6O_{55}]^{q-}$ polyfluoroxometalate anion where the transition metal (TM) is in the α_1 "belt" position (see below). Na, green; H, gray; TM, blue; W, black; F, yellow; O, red.

a subclass of the analogous polyoxometalate compounds, where an electron withdrawing but π-donating fluorine atom is an axial ligand to the substituted transition metal and *trans* to the purported reaction site. These polyfluoroxometalates have been only sparsely studied, for example, as epoxidation catalysts with H_2O_2 (TM = Ni(II))[13] and as catalysts for aerobic hydroxylation and oxidative dehydrogenation of alkylated arenes (TM = V(V)).[14] Their investigation in the context of stabilization of high valent species in water not been reported nor has there been a study of their reactivity.

In the research presented below we present the synthesis and characterization of a series of manganese substituted polyfluoroxometalate anions, $[NaH_2(Mn\text{-}L)W_{17}F_6O_{55}]^{q-}$ where Mn-L is Mn(II)-H_2O, Mn(III)-H_2O, Mn(IV)-OH and Mn(V)-OH. Furthermore, we present the quite surprising reactivity profiles in water of the Mn(IV)-OH and Mn(V)-OH containing compounds. Both are very effective in electron transfer oxidation but are surprisingly very poor oxygen-atom donors. The Mn(V)-OH compound is stable in water, while the Mn(IV)-OH compound reacts to yield O_2. In the latter reaction we have observed a strong catalytic effect of alkali cations that is explained by formation of aggregates in solution and shows the possible viability of a tetra Mn(IV)-OH intermediate as an oxygen forming species.

RESULTS AND DISCUSSION

Synthesis and Characterization. The manganese(II) substituted polyfluoroxometalate with an aqua ligand at the terminal position, Figure 1, where TM = Mn(II), $K_9[NaH_2Mn(II)(H_2O)W_{17}F_6O_{55}]$, Mn(II)PFOM was known from the literature.[13] The procedure for its synthesis involves first the preparation of the analogous zinc substituted compound, $K_9[NaH_2Zn(II)(H_2O)W_{17}F_6O_{55}]$, (Zn(II)PFOM) followed by metathetical exchange of Zn(II) with Mn(II). In principle, the Zn/Mn atom may occupy an α_1 "belt" or an α_2 "capped" position. In a novel observation reported here, we found that in the initial preparation of Zn(II)PFOM, the formation of only the α_1 isomer can be assured by carefully controlling the temperature of the preparation to 80−85 °C; lower temperatures lead to some formation of the α_2 isomer. This indicates that the α_1 isomer is thermodynamically favored. The ^{19}F NMR spectral analysis and peak assignment with $^1H/^{19}F$ 2D HETCOR NMR are presented in the Supporting Information, Figures S1−S3. It was assumed that after the metathetical exchange of Zn(II) with Mn(II) the α_1 isomer is retained. Interestingly, based on research on metathetical exchange of Zn(II) with other metals it was discovered by NMR experiments that for a Co(III) substituted compound there can exist both a dimeric and monomeric form.[15] The paramagnetism of Mn(II)PFOM precludes such a NMR analysis in this case, but we were able to crystallize some of the dimer. The structure obtained by X-ray diffraction, Figure S4, clearly shows that the substitution of Mn(II) is in the α_1 "belt" position. Additional oxidation states of manganese, III, IV and V, are accessible as presented in Scheme 1 by oxidation with peroxodisulfate, $S_2O_8^{2-}$. As will be shown below, only monomers of these compounds were obtained.

Scheme 1. Preparation of Manganese Substituted Polyfluoroxometalates

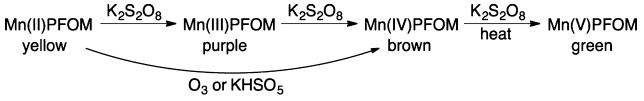

The efficient formation of Mn(V)PFOM requires elevated temperatures, and the synthesis of Mn(IV)PFOM is more practical using ozone or monopersulfate, HSO_5^-, delivered as the triple salt, Oxone. The manifestation of the different colors can be observed in the UV−vis spectra, Figure 2.

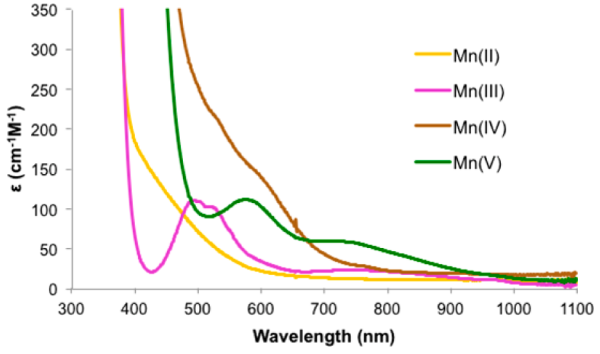

Figure 2. UV−vis spectra of the various manganese substituted polyfluoroxometalates, 3.4 mM in water. Peaks: Mn(III)PFOM, 493, 521, 746 nm; Mn(IV)PFOM, 540 (sh), 615 (sh) nm; Mn(V)PFOM – 576, 718 nm.

In order to confirm that the monomeric quasi Wells−Dawson structure of the polyfluoroxometalates was retained during the oxidation reactions, single crystal X-ray diffraction measurements were made. The crystal structures, Figure S5, see also the cif files in the Supporting Information, clearly show that indeed the original basic structure was unchanged as shown in Figure 1 although there is a disorder of the location of manganese in the α_1 "belt" position preventing clear identification of the terminal ligand by this method. This also prevents the determination of the manganese oxidation state, and of course spin state, by X-ray diffraction through bond

DOI: 10.1021/jacs.5b03456
J. Am. Chem. Soc. 2015, 137, 8738−8748

valence sum (BVS) analysis. However, this information can be obtained from XPS and XAS (XANES and EXAFS) and magnetic susceptibility measurements.

The XPS data are summarized in Figure 3 where the difference in binding energies between the Mn $2p^{3/2}$ and W

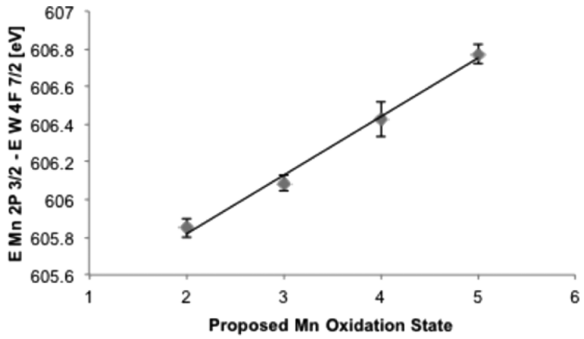

Figure 3. Corrected binding energies of Mn $2p^{3/2}$ as a function of the oxidation state of manganese.

$4f^{7/2}$ orbitals, Mn $2p^{3/2}$ − W $4f^{7/2}$, is presented; more details can be found in Figure S6. This data presentation was carried out to rectify charging effects implicit to the XPS technique, which gives reliable corrected binding energies under the realistic assumption that the binding energy of the W $4f^{7/2}$ electrons do not change as a function of the oxidation state of manganese. As one may observe, an excellent linear correlation between the corrected binding energy and the proposed oxidation state of manganese; a difference of ∼0.31 eV in binding energy between each oxidation state was found.

X-ray absorption spectroscopic measurements were made as well in order to verify the assignment of the manganese oxidation state in the MnPFOM series and gain some structural insight. The X-ray absorption near-edge structure (XANES) spectra of the four MnPFOM complexes are shown in Figure 4

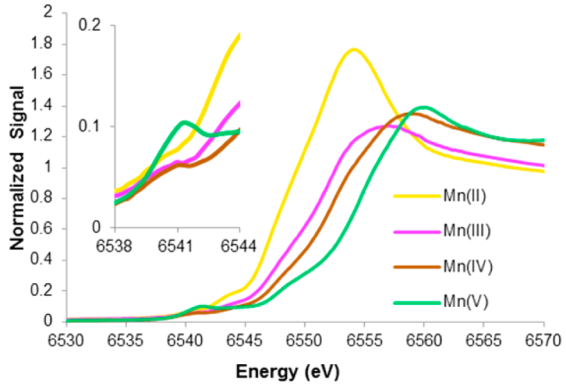

Figure 4. Mn K-edge XANES of MnPFOM species measured at 30 K. Inset: Pre-edge areas of the MnPFOM species.

and the corresponding properties are summarized in Table 1. Visual examination of the spectra reveals the edge energy increasing from Mn(II)PFOM to Mn(V)PFOM; a more quantitative analysis of the data indicates a 2 to 3 eV step for each increment in the Mn oxidation state. As in the case of the XPS measurements, there is a very good linear correlation between the oxidation state of manganese and the K-edge energy, Figure S7. Such a trend has been previously reported

Table 1. Mn K-Edge XANES and EXAFS Data for the MnPFOM Series (E_0 = 6539 eV for Mn Metal)[a]

	E_0, eV	$E_{pre\text{-}edge}$, eV	pre-edge area	Best EXAFS fits
Mn(II)	6547.0	6540.1	1.6	6O @ 2.13 Å
Mn(III)	6550.3	6540.2	3.5	3O @ 1.93 Å[b]
				2O @ 2.20 Å
Mn(IV)	6552.4	6540.6	7.7	4O @ 1.92 Å
				2O @ 2.23 Å
Mn(V)	6554.5	6541.1	15.4	1O @ 1.78 Å
				4O @ 1.92 Å
				1O @ 2.30 Å

[a]Mn K-edge energies for MnO (6546.2 eV), Mn_2O_3 (6550.1 eV) and MnO_2 (6553.5 eV) have been reported.[19] [b]The best fit uses only five scatterers. This is well within the standard error of 25% for determining coordination numbers and is fully consistent with a 6-coordinate Mn center for the whole series.

for a series of manganese oxides, MnO, Mn_3O_4 Mn_2O_3, and MnO_2.[16]

In contrast to the K-edge energies, the pre-edge features before the main K-edge crest provide different insights into the nature of each Mn center in the series. These features correspond to crystal field transitions from the core 1s levels to the half-occupied or empty 3d levels, which can gain some 4p character depending on the extent of deviation from centrosymmetry.[17] Thus, complexes with more distorted geometries exhibit larger pre-edge areas than the complexes with less distorted geometries. A 50:50 pseudo Voigt function was utilized to model both the rising edge and the peak so as to get the pre-edge area value, Table 1 and Figure S8. The data in Table 1 show that all the MnPFOM species share a pre-edge peak at 6540.6 ± 0.5 eV, which increases in area with the Mn oxidation state.[18] The 10-fold increase in the pre-edge peak area observed on going from Mn(II) to Mn(V) likely reflects a growing distortion from octahedral symmetry as the Mn center gets higher in oxidation state.

EXAFS data were collected and analyzed for all four complexes in the series. The best fits are listed in Table 1; more detailed analysis and the spectra may be found in the Supporting Information, Figures S9−S12. Since the atomic mass and size between O and F are quite similar it is not possible to differentiate the scatters between them from the EXAFS data. Thus, the spectrum of Mn(II)PFOM is best fit with one shell of 6 O scatterers at 2.13 Å (Figure S9). These bond lengths are consistent with bond lengths observed in first row transition metal substituted polyoxometalates where the transition metal is in the same nearest neighbor environment, such as $[ZnW(MnH_2O)_2(ZnW_9O_{34})_2]^{12-19}$ This result, together with the observation that this complex has the smallest pre-edge area of the series, is consistent with a highly symmetric octahedral center, as expected for a high-spin d^5 Mn(II) center. On the other hand, Mn(III)PFOM should exhibit a Jahn−Teller distortion and is best fit with two subshells of O atoms at 1.93 and 2.20 Å (Figure S10). Mn(IV)PFOM is best fit with 4 O scatterers at 1.92 Å and 2 O scatterers at 2.23 Å (Figure S11). That an O scatterer at 1.7 Å is not required to obtain a good fit excludes the possibility of a Mn═O unit being present in this complex.[20] The pre-edge area of Mn(IV)PFOM sample is 7.7, which also suggests that the Mn ligand environment is not very distorted from centrosymmetry, unlike what might be expected for a Mn═O complex. Lastly, Mn(V)PFOM is best fit with an O atom at

DOI: 10.1021/jacs.5b03456
J. Am. Chem. Soc. 2015, 137, 8738−8748

1.78 Å, 4 O atoms at 1.92 Å, and an O atom at 2.30 Å (Figure S12). These results also exclude the possibility of a Mn(V)=O unit, which is expected to have a bond length of about 1.6 Å;[21] instead, the 1.78 Å O scatterer of the best fit would appear to point to the presence of a Mn(V)-OH unit.[18] An authentic Mn(V)-hydroxo compound has apparently not yet been prepared, but in our experience it would not be surprising for the oxygen-rich PFOM ligand environment to support such a high-valent unit.

The magnetic susceptibilities of the various MnPFOM compounds as solids were measured at room temperature using a magnetic balance. Magnetic susceptibility was also measured during cooling and heating of the samples at $2 \leq T \leq 300$ K at H = 5000 Oe using a SQUID magnetometer, Figure S13. The data were fitted well using the Curie equation at 100–300 K. Most importantly, the data clearly show that the compounds are high spin, Table 2.[22]

Table 2. Results of Magnetic Measurements of MnPFOM[a]

	S	g	$g\sqrt{(S(S+1))}$, BM	μ_{eff}, BM[b]
Mn(II)	5/2	2.0[c]	6.21	5.7
Mn(III)	2	1.87	4.58	4.6
Mn(IV)	3/2	2.06	4.01	3.9
Mn(V)	1	2.58	3.64	3.2

[a]Other S values gave calculated g-factors that were much farther from $g = 2$, indicating that the given S values best fit the data, see Table S1. [b]Room temperature measurement with magnetic balance. [c]Set at $g = 2$ after measurement of the EPR spectrum indicating so.

Reactivity. The water-soluble Mn(IV)-OH-PFOM and Mn(V)-OH-PFOM compounds were investigated with respect to their reactivity in O atom transfer, electron transfer oxidation, and formation of O_2 as related to water oxidation. Within this context, it is important to keep in mind that Mn(IV)-OH-PFOM reacts very fast (<1 s) with Mn(II)-H_2O-PFOM; Mn(V)-OH-PFOM does not react with Mn(III)-H_2O-PFOM and Mn(V)-OH-PFOM reacts rather slowly, $t_{1/2}$= 6.5 min, with Mn(II)-H_2O-PFOM (eqs 1– 3).

$$\text{Mn(IV)-OH-PFOM} + \text{Mn(II)-H}_2\text{O-PFOM} \rightarrow 2\text{Mn(III)-H}_2\text{O-PFOM} \quad (1)$$

$$\text{Mn(V)-OH-PFOM} + \text{Mn(III)-H}_2\text{O-PFOM} \not\rightarrow 2\text{Mn(IV)-H}_2\text{O-PFOM} \quad (2)$$

$$\text{Mn(V)-OH-PFOM} + 2\text{Mn(II)-H}_2\text{O-PFOM} \rightarrow 3\text{Mn(III)-H}_2\text{O-PFOM} \quad (3)$$

O atom transfer to the water-soluble phosphine $(Na^+/^-O_3SC_6H_4)_3P$ to form the corresponding phosphine oxide $(Na^+/^-O_3SC_6H_4)_3P{=}O$ with the two manganese hydroxo species showed significant differences. A reaction of a 3.3 mM solution of Mn(IV)-OH-PFOM with 1 equiv of $(Na^+/^-O_3SC_6H_4)_3P$ at room temperature was quickly completed with a $t_{1/2}$ = 0.5 s with a ∼50% yield of $(Na^+/^-O_3SC_6H_4)_3P{=}O$, Figure S14. On the other hand, a reaction of a 3.3 mM solution of Mn(V)-OH-PFOM with 1 equiv of $(Na^+/^-O_3SC_6H_4)_3P$ at room temperature was very slow ($t_{1/2}$ = ∼1 h) and yielded ∼100% $(Na^+/^-O_3SC_6H_4)_3P{=}O$. One can conclude that these reactions occur according to eqs 4 and 5, respectively. Despite the fast oxygenation of the phosphine with Mn(IV)-OH-PFOM, this compound was surprisingly inert in the oxidation of water-soluble substrates such as dimethyl sulfoxide to dimethylsulfone or allyl alcohol to the corresponding epoxide. More obviously Mn(V)-OH-PFOM was also not reactive to these substrates. Clearly, both hydroxo compounds can be considered inferior O atom donors to organic substrates. The very low reactivity of the Mn(V) species supports the assignment of the compound as having a terminal OH ligand, Mn(V)-OH-PFOM. In contrast, a Mn(V)-oxo species in another polyoxometalate framework and in organic solvent[11] have been shown to be quite reactive.

$$\text{Mn(IV)-OH-PFOM} + (Na^+PhSO_3^-)_3P \rightarrow \text{Mn(II)-H}_2\text{O-PFOM} + (Na^+PhSO_3^-)_3P{=}O$$

$$\text{Mn(IV)-OH-PFOM} + \text{Mn(II)-H}_2\text{O-PFOM} \rightarrow 2\text{Mn(III)-H}_2\text{O-PFOM} \quad (4)$$

$$\text{Mn(V)-OH-PFOM} + (Na^+PhSO_3^-)_3P \rightarrow \text{Mn(III)-H}_2\text{O-PFOM} + (Na^+PhSO_3^-)_3P{=}O \quad (5)$$

Mn(IV)-OH-PFOM and Mn(V)-OH-PFOM were also tested as electron transfer oxidants. In the outer sphere oxidation of potassium ferrocyanide, the data show (see Supporting Information, Figure S15) that the reaction of 3.3 mM Mn(V)-OH-PFOM with 1 equiv of ferrocyanide was about 40 times faster than the analogous reaction with Mn(IV)-OH-PFOM (eqs 6 and 7).

$$\text{Mn(V)-OH-PFOM} + K_4[\text{Fe(II)CN}_6] \xrightarrow{t_{1/2}\sim 0.4\ \text{sec}} \text{Mn(IV)-OH-PFOM} + K_3[\text{Fe(III)CN}_6] \quad (6)$$

$$\text{Mn(IV)-OH-PFOM} + K_4[\text{Fe(II)CN}_6] \xrightarrow{t_{1/2}\sim 15\ \text{sec}} \text{Mn(III)-H}_2\text{O-PFOM} + K_3[\text{Fe(III)CN}_6] \quad (7)$$

A different outcome however was observed in the oxidation of 3-mercaptopropionic acid, RSH (R = CH_2CH_2COOH) to the corresponding disulfide. The formation of disulfide was verified and quantified by ^{1}H NMR, while the reaction kinetics were measured by UV–vis spectroscopy. The reaction of Mn(V)-OH-PFOM (3.3. mM) with 2 equiv of RSH had a $t_{1/2}$ = 8.8 s and afforded RSSR and Mn(III)-H_2O-PFOM in ∼100% yield. In contrast, the oxidation of RSH by Mn(IV)-OH-PFOM under similar conditions was an order of magnitude faster with $t_{1/2}$ = 0.8 s to yield RSSR in a ∼50% yield and Mn(III)-H_2O-PFOM. The latter reacted very slowly over 48 h wherein the remaining RSH was also oxidized to RSSR to and formed Mn(II)-H_2O-PFOM. The stoichiometry and reactivity are summarized in eqs 8 and 9.

$$\text{Mn(V)-OH-PFOM} + 2\text{RSH} \xrightarrow{t_{1/2}\sim 8.8\ \text{sec}} \text{Mn(III)-H}_2\text{O-PFOM} + \text{RSSR} \quad (8)$$

DOI: 10.1021/jacs.5b03456
J. Am. Chem. Soc. 2015, 137, 8738–8748

$$\text{Mn(IV)-OH-PFOM} + 2\text{RSH} \xrightarrow{t_{1/2}\sim 0.8\ \text{sec}} \text{Mn(III)-H}_2\text{O-PFOM} + 1/2\text{RSSR} + \text{RSH}$$

$$\text{Mn(III)-H}_2\text{O-PFOM} + \text{RSH} \xrightarrow{48\ \text{h}} \text{Mn(II)-H}_2\text{O-PFOM} + 1/2\text{RSSR} \quad (9)$$

The difference in the reactivity of Mn(IV)-OH-PFOM and Mn(V)-OH-PFOM in these two electron transfer reactions can be explained as follows: The oxidation of ferrocyanide is a classic example of an outer sphere reaction and therefore the compound with the higher potential, Mn(V)-OH-PFOM, reacts more quickly.[23] On the other hand, the thiol oxidation is more likely to be an inner sphere reaction requiring thiolate coordination at the metal center. Thus, ligand exchange between the thiol and bound hydroxide should precede the electron transfer step. As the terminal Mn-OH bond of Mn(IV)-OH-PFOM is expected to be slightly longer and weaker than that of Mn(V)-OH-PFOM, the reaction is more facile for the former.

During the preparation of the Mn(IV)-OH-PFOM and Mn(V)-OH-PFOM compounds it was noticed that Mn(IV)-OH-PFOM tended to be slowly reduced in water to yield Mn(III)-H_2O-PFOM, while Mn(V)-OH-PFOM was indefinitely stable. This suggested that Mn(IV)-OH-PFOM might have reacted in water to yield an oxidized product. Thus, 0.4 mL of 46 mM Mn(IV)-OH-PFOM in double distilled water were inserted into a 2 mL vial and sealed with a septum. The vial was then purged with CO_2 for 10 min in order to remove all air. 120 μL of N_2O were inserted to the vial as an internal standard. The vial was left overnight at 70 °C to react. Finally, the amount of O_2 in the gas phase of the vial was quantified by gas chromatography by integrating the peak area of O_2 versus that of N_2O. Indeed for every mol of Mn(IV)-OH-PFOM the formation of ~0.25 mol O_2 was observed and a balanced equation would indicate the following reaction stoichiometry, eq 10.

$$4\text{Mn(IV)-OH-PFOM} + 2\text{H}_2\text{O} \rightarrow 4\text{Mn(III)-H}_2\text{O-PFOM} + \text{O}_2 \quad (10)$$

The formation of O_2 from Mn(IV)-OH-PFOM stands in sharp contrast to its low reactivity as a oxygen atom donor. Further investigation showed that the addition of salts, originally KCl, had a strong effect on the rate of formation of O_2 and formation of Mn(III)-H_2O-PFOM from Mn(IV)-OH-PFOM. Reaction profiles measured by UV−vis spectrometry at 80 °C in the presence of various alkali metal cations by the disappearance of Mn(IV)-OH-PFOM are presented in Figure 5, bottom. Although the reaction in its entirety is not very fast, the catalytic effect $Cs^+ > Rb^+ > K^+ > Na^+ \sim$ none $\sim Li^+$ is striking. Another notable feature is the change in the reaction order in Mn(IV)-OH-PFOM. Plotting, Figure 5, top, ln(rate) = ln(−d[Mn(IV)-OH-PFOM]/dt) versus ln([Mn(IV)-OH-PFOM] gives the slopes as the reaction order in Mn(IV)-OH-PFOM, which are ~2 in the presence of KCl, and ~4 in the presence of CsCl.

It is well-known that the solubility of polyoxometalates tends to decrease as one goes from Li to Cs counter cations.[24] This fact led us to investigate the possibility that perhaps colloid clusters of polyoxometalates are being formed in solution. Note that the solutions are completely transparent to the naked eye

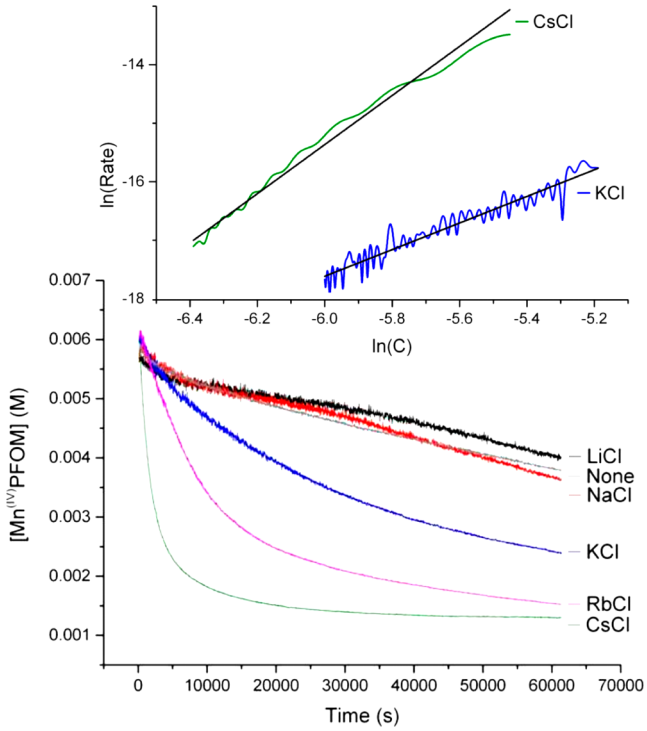

Figure 5. Bottom: Profiles of the reaction of 4.5 mM Mn(IV)-OH-PFOM in the presence of 70 mM of MCl (M = Li, Na, K, Rb or Cs) at 80 °C. KF yielded essentially the same result as KCl and KBr was oxidized to Br_2. Top: ln/ln plots of the reaction rates versus concentration generated from the reaction profiles. Experimental data (colored) and linear fit (black). Slope: KCl = 2.2; CsCl = 4.1. Note that the noise in the UV−vis measurement is amplified in the data manipulation.

and remain so at the reaction temperature of 80 °C, meaning that there are no particles >500 nm in size. Formation of clusters could facilitate the O_2 forming reactions since having the reaction centers in close proximity would obviously be important in a multicentered, multielectron reaction. Such formation of clusters could change the free energy, enthalpy and entropy of activation of the reaction and also the reaction mechanism. Since the reaction orders are different in the presence of the different cations, it is difficult to make highly accurate comparisons of the activation parameters. Despite this Eyring plots of reactions, Figure S17, in the presence of KCl and RbCl gave the following activation parameters assuming second order reactions:

KCl: $\Delta H^{\ddagger} = 65 \pm 2$ kJ/mol;
$\Delta S^{\ddagger} = -104 \pm 6$ J/mol K;
$\Delta G^{\ddagger}_{298} = 96 \pm 7$ kJ/mol

RbCl: $\Delta H^{\ddagger} = 41 \pm 2$ kJ/mol;
$\Delta S^{\ddagger} = -168 \pm 6$ J/mol K;
$\Delta G^{\ddagger}_{298} = 92 \pm 5$ kJ/mol

Clearly for RbCl the $\Delta S^{\ddagger}$ is considerably lower than the $\Delta S^{\ddagger}$ observed for KCl, although the $\Delta G^{\ddagger}_{298}$ of both reactions are the same within the experimental error of the measurement. One may conclude that the transition state is more ordered in the series $Cs^+ > Rb^+ > K^+ > Na^+ \geq Li^+$. The activation parameters for the Cs^+ case could not be measured because of precipitate

DOI: 10.1021/jacs.5b03456
J. Am. Chem. Soc. 2015, 137, 8738−8748

formation at lower temperatures and a large deviation from second order.

In order to evaluate if clusters are indeed being formed in the reaction solution and taking to advantage the high contrast the presence of tungsten atoms provide, cryo transmission and cryo scanning-transmission electron microscopy (TEM) and (STEM) measurements were made to directly observe the polyoxometalatate in solution. The solutions were heated to 60 °C, and flash-frozen directly, thus preserving the experimental conditions. Figures 6 and 7 present STEM and TEM images,

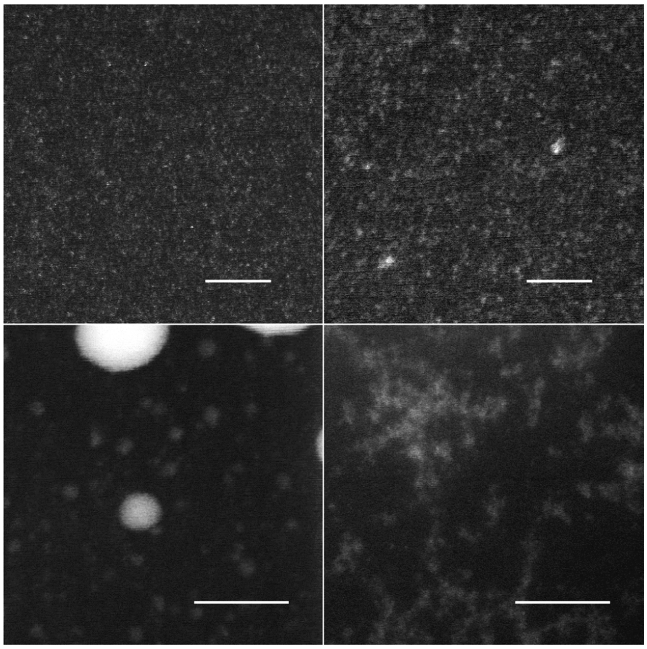

Figure 6. Cryo-STEM pictures from solutions of 4.5 mM Mn(IV)-OH-PFOM and 70 mM of MCl. M = Li (top left), Na (top right), K (bottom left), and Cs (bottom right) at 60 °C. Scale bar is 50 nm, white is high contrast.

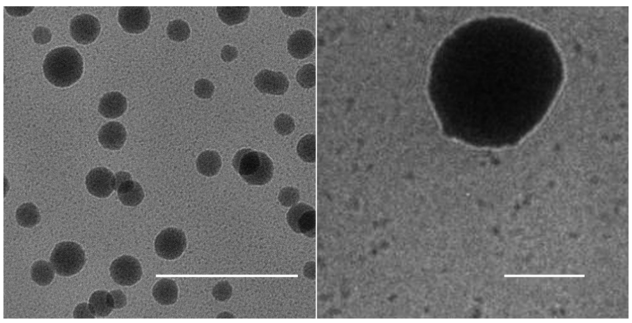

Figure 7. Cryo-TEM pictures from solutions of 4.5 mM Mn(IV)-OH-PFOM and 70 mM of MCl. M = K (left), and Cs (right) at 60 °C. Scale bar is 200 nm, dark is high contrast.

respectively, that clearly show differences in the arrangement of polyoxometalates in frozen vitreous glass solution. The TEM shows the large particles while STEM was used to survey the space between the larger particles. The solutions prepared in the presence of LiCl are completely homogeneous with no evidence for the formation of any clusters. Solutions containing NaCl are quite similar with perhaps formation of some very small assemblies. On the other hand, Mn(IV)-OH-PFOM in the presence of KCl leads to the observation of small colloidal particles, that is 2−5 nm and larger particles of ∼50 nm. In the presence of CsCl two different types of structures are observable: dendrite type structures that are more easily viewed by STEM and large spherical colloids that can be seen by TEM.

Some of the colloidal particles formed from 4.5 mM Mn(IV)-OH-PFOM with 70 mM of CsCl are sufficiently large so that a relatively accurate EDX measurement can be made using cryo-STEM. The results, Figure S18, show that these colloid particles are indeed composed of polyoxometalate anions with the surrounding Cs cations and water.

In order to support the observation of large polyoxometalate assemblies in solution by an entirely different technique, diffusion NMR, DOSY, was used to approximate particle size.[25] In this measurement we focused on the hydrogen atom inside the PFOM structure, Figure 1. Since Mn(IV)-OH-PFOM is paramagnetic and shows no NMR signal, the isostructural diamagnetic Zn(II)PFOM was used instead. The results shown in Figure 8 reveal that in the presence of LiCl or NaCl, particles

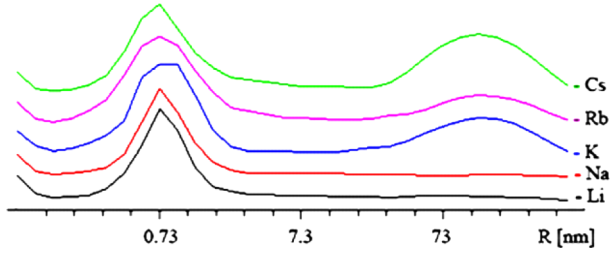

Figure 8. Size distributions obtained from DOSY NMR experiments. The solutions were 4.5 mM Zn(II)PFOM and 70 mM of MCl (M = Li, Na, K, Rb or Cs) at 80 °C in D_2O.

in the one-nanometer region are present. Since the Zn(II)-PFOM polyoxometalate itself has such nanometric dimensions, the DOSY experiment supports the electron microscope observation showing the absence of aggregates and the absence of a catalytic effect for O_2 formation in the presence of LiCl or NaCl, Figure 6. On the other hand when KCl, RbCl or CsCl are added to Zn(II)PFOM in water there is a bimodal distribution that varies according to the alkali cation added. In addition to the single Zn(II)PFOM molecules present in all cases for K^+, one can see particles ranging from ∼10 to 100 nm. For Cs^+, the larger aggregates are clearly present, although it appears that only few aggregates in the 10−50 nm region are formed. The Rb^+ cation shows intermediate behavior. It should be noted that the analysis of DOSY data is based on the assumption that spherical particles are formed; the EM data clearly show that also dendritic aggregates are present. Therefore, although the DOSY experiments support the observation of aggregates or colloids in the presence of KCl, RbCl or CsCl, it is likely a poor indicator of the actual size distribution of the larger particles.

There are several points worth emphasizing concerning the reactivity profiles of Mn(V)-OH-PFOM and Mn(IV)-OH-PFOM in general and more specifically the O_2 formation reaction that was observed from Mn(IV)-OH-PFOM.

Mn(V)-OH-PFOM: This higher oxidation state and high spin compound (S = 1), which is very stable in the solid state and in water, is a very poor O atom donor even to highly reactive phosphines. On the other hand, it has a sufficiently high oxidation potential for the very fast outer-sphere electron transfer oxidation of ferricyanide and the somewhat slower inner sphere electron transfer oxidation of a water-soluble thiol

DOI: 10.1021/jacs.5b03456
J. Am. Chem. Soc. 2015, 137, 8738−8748

to yield the corresponding disulfide. It showed no formation of O_2 and was very stable in water. Since this seems to be the first such Mn(V)-OH species that has been reported it is presently difficult to put this low reactivity in a broader perspective.

Mn(IV)-OH-PFOM: The high spin Mn(IV)-OH-PFOM compound is a somewhat better O atom donor, although its reactivity appears to be limited to phosphines. It is a weaker outer sphere electron transfer oxidant, but in the electron transfer oxidation of 3-mercaptopropionic acid to the corresponding disulfide it is more reactive than Mn(V)-OH-PFOM presumably because it is an inner sphere oxidation, requiring ligand exchange. The formation of O_2 in water from Mn(IV)-OH-PFOM is especially interesting. As Mn(III)-H_2O-PFOM is the reaction product 4 equiv of Mn(IV)-OH-PFOM are needed to form 1 equiv of O_2 as shown in eq 10. In a bimolecular mechanism two simple scenarios can be envisioned, Scheme 2. Assuming Mn(IV)-OH-PFOM is a one

Scheme 2. Conceivable Pathways for Formation of O_2

Bimolecular Pathway

A $2\ \text{Mn(IV)-OH-PFOM} + 2\ H_2O \xrightarrow{\text{rds}} 2\ \text{Mn(III)-}H_2\text{O-PFOM} + H_2O_2$

$2\ \text{Mn(IV)-OH-PFOM} + H_2O_2 \xrightarrow{\text{fast}} 2\ \text{Mn(III)-}H_2\text{O-PFOM} + O_2$

B $2\ \text{Mn(IV)-OH-PFOM} + 2\ H_2O \xrightarrow{\text{rds}} 2\ \text{Mn(II)-}H_2\text{O-PFOM} + O_2 + 2\ H^+$

$2\ \text{Mn(IV)-OH-PFOM} + 2\ \text{Mn(II)-}H_2\text{O-PFOM} + 2\ H^+ \xrightarrow{\text{fast}} 4\ \text{Mn(III)-}H_2\text{O-PFOM}$

Tetramolecular Pathway

C $4\ \text{Mn(IV)-OH-PFOM} + 2\ H_2O \xrightarrow{\text{rds}} 4\ \text{Mn(III)-}H_2\text{O-PFOM} + O_2$

electron oxidant one can propose that H_2O_2, which was not detectable, is formed in the rate-determining step and is then decomposed quickly, as was separately observed, with additional Mn(IV)-OH-PFOM to yield O_2, pathway A. Alternatively, Mn(IV)-OH-PFOM could be a two-electron oxidant, yielding O_2 in one step and Mn(II)-H_2O-PFOM, pathway B. The latter would react very fast with Mn(IV)-OH-PFOM by comproportionation, eq 1, to yield Mn(III)-H_2O-PFOM. When Mn−Mn distances are on the average large this would be the expected reaction mechanism. The reactivity of Mn(IV)-OH-PFOM does not support a recent suggestion that initial O−O bond formation with the oxygen evolving complex does not involve an Mn^{IV}-OH unit.[8j]

The reactivity of Mn(IV)-OH-PFOM in the presence heavier alkali metal salts, such as CsCl is especially noteworthy taking into account the considerable rate enhancement observed and the fourth order reaction in Mn(IV)-OH-PFOM.[26] The well accepted Kok cycle[27] proposes the formation of O_2 from the yet to be isolated or directly observed highly reactive S_4 state of the tetramanganese cluster, that is the oxygen evolving complex (OEC) of PSII.[3,28] There appears to still be debate concerning the oxidation states of manganese in S_4 although a tetra-Mn(IV) complex appears most likely for S_3.[28] From this research one could hypothesize that a four centered Mn(IV)-OH-PFOM arrangement could be possible through colloid formation of Mn(IV)-OH-PFOM in the presence of heavier alkali metals. This would allow formation of O_2 from an S_4 like OEC involving four molecules of Mn(IV)-OH-PFOM, Scheme 2, pathway C. In order to see if such a hypothesis is reasonable in an intermolecular assembly, in Figure 9 we present a TEM image of a colloid where on the edge of the sphere one can observe a high degree of ordering of the PFOM molecules, which have a ∼1 nm cross-section, within the colloidal structure. Furthermore, in Figure 10 we present the Mn−Mn

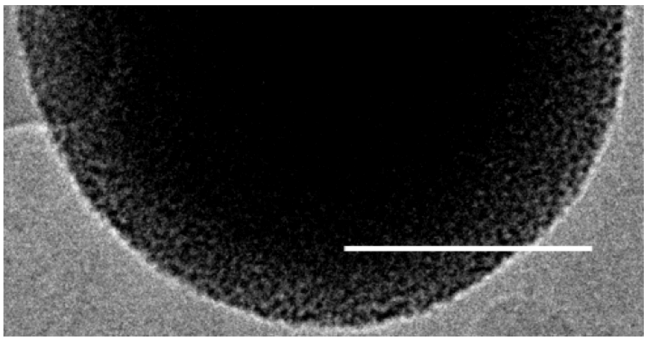

Figure 9. A zoom in on a cryo-TEM image of a colloid particle of Mn(IV)-OH-PFOM. Scale bar = 50 nm.

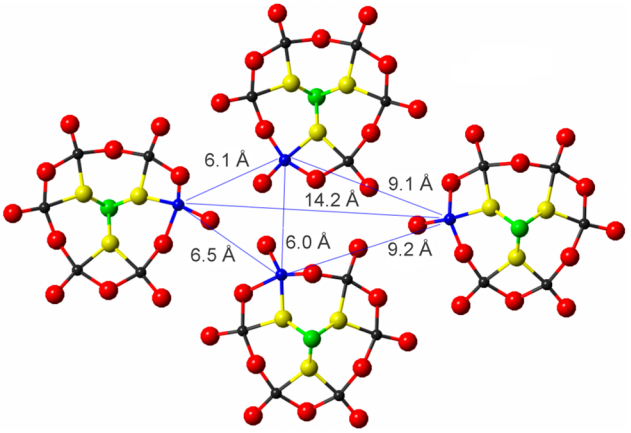

Figure 10. Possible intermolecular Mn−Mn distances in the crystal of $K_8[NaH_2Mn(IV)(OH)W_{17}F_6O_{55}]\cdot 15H_2O$ considering optimal organization of 4 PFOM molecules.

distances as can be deduced from the crystal structure of Mn(IV)-OH-PFOM. Clearly the Mn−Mn distances are significantly longer in such an intermolecular assembly than the distances, <3 Å, known for the OEC unit. For an O−O bond to be formed either some H_2O and cations would need to be "squeezed" out of the interstitial space between the Mn atoms or some Mn(IV)-OH species could reversibly migrate from the PFOM to the interstitial space. However, and perhaps paradoxically, these longer Mn−Mn distances slow down the O_2 formation reaction considerably allowing its observation from a complex, Mn(IV)-OH-PFOM, that has been well characterized. In this way we can conclude that a high spin tetra-Mn(IV)-OH OEC can be considered as a viable, but of course not proven, possibility for the OEC, and also would be an interesting target for synthetic oxide based analogs of a water oxidation catalyst.

CONCLUSIONS

A manganese(II)-substituted polyfluoroxometalate was used as a synthetic platform for the isolation of four different high spin species, Mn(II)-H_2O-PFOM, Mn(III)-H_2O-PFOM, Mn(IV)-OH-PFOM, and Mn(V)-OH-PFOM as determined from magnetic susceptibility, XPS and XAS (XANES and EXAFS) measurements. The coordination environment around manganese for the Mn(IV)-OH-PFOM and Mn(V)-OH-PFOM has four oxygen atoms in the equatorial plane, an accessible axial hydroxo terminal ligand and an inaccessible fluorine atom *trans* to the hydroxo ligand. It would appear that the fluorine

DOI: 10.1021/jacs.5b03456
J. Am. Chem. Soc. 2015, 137, 8738−8748

Table 3. Crystallographic Data for Compounds Mn(II)-PFOM, Mn(III)-PFOM, Mn(IV)-PFOM, and Mn(V)-PFOM

	Mn(II)PFOM	Mn(III)-PFOM	Mn(IV)-PFOM	Mn(V)-PFOM
formula	$F_{12}Mn_2O_{110}W_{34}Na_2$ 40O 18K	$F_6MnO_{56}W_{17}Na$ 13O 9K	$F_6MnO_{56}W_{17}Na$ 15O 9K	$F_6MnO_{56}W_{17}Na$ 20O 8K
formula weight (g mol^{-1})	9738.56	4760.39	4805.28	4846.18
crystal system	monoclinic	triclinic	monoclinic	triclinic
space group	$C2/c$	$P\bar{1}$	$C2/c$	$P\bar{1}$
T (K)	100(2)	100(2)	120(2)	100(2)
a (Å)	43.248(9)	12.2907(7)	22.604(5)	12.2185(13)
b (Å)	12.198(2)	12.8548(7)	12.289(3)	12.8189(13)
c (Å)	29.370(6)	29.2936(16)	29.349(6)	13.5340(15)
α (deg)	90.00	87.980(2)	90.00	104.662(5)
β (deg)	101.13(3)	90.005(2)	92.40(3)	90.032(5)
γ (deg)	90.00	61.462(2)	90.00	118.350(5)
V (Å^3)	15202(5)	4062.6(4)	8145(3)	1786.6(3)
Z	4	2	4	1
D_{calc} (g cm^{-3})	4.255	3.891	3.918	4.504
μ (mm^{-1})	26.394	24.630	24.623	28.016
collected reflections	85127	33331	8278	13985
reflections $[I > 2\sigma(I)]$	10224	18455	7539	13537
R_{int}	0.0655	0.0514	0.0509	0.0449
parameters/restraints	1001/108	934/116	522/43	1035/166
$R(F)^a$ $[I > 2\sigma(I)]$	0.0572	0.0577	0.0506	0.0359
$wR(F^2)^a$ (all data)	0.1555	0.1576	0.1341	0.0884
GOF	1.093	1.031	1.084	1.047

$^a(F) = \Sigma||F_o - F_c||/\Sigma|F_o|$. $wR(F^2) = \{\Sigma[w(F_o^2 - F_c^2)^2]/\Sigma[w(F_o^2)^2]\}^{1/2}$.

atom as an electron-withdrawing, but π-donating ligand plays a key role in the stabilization of Mn(IV)-OH-PFOM and Mn(V)-OH-PFOM. Both Mn(IV)-OH-PFOM and Mn(V)-OH-PFOM in water were found to be poor oxygen atom donors, although the Mn(IV)-OH-PFOM oxidized $(Na^+/^-O_3SC_6H_4)_3P$ to $(Na^+/^-O_3SC_6H_4)_3P{=}O$ at room temperature within a few seconds ($t_{1/2}$ = 0.5 s). The analogous reaction with Mn(V)-OH-PFOM was much slower, $t_{1/2}$ = 1 h. Both Mn(IV)-OH-PFOM and Mn(V)-OH-PFOM were reactive as one-electron oxidants. The results show that Mn(V)-OH-PFOM is the better outer sphere oxidant with ferrocyanide as the substrate as would be expected for a higher valent species. On the other hand Mn(IV)-OH-PFOM was more reactive in what appears to be an inner sphere oxidation of 3-mercaptopropionic acid that requires nucleophilic substitution of the terminal hydroxo ligand that is less strongly bonded in Mn(IV)-OH-PFOM.

The formation of O_2 from Mn(IV)-OH-PFOM is the most notable aspect related to reactivity in this research. The O_2 formation reaction is catalyzed by the presence of alkali metal cations, K^+, Rb^+ and Cs^+. The catalytic effect is due to formation of aggregates that were of a dendritic and colloidal nature as visualized by cryo STEM and cryo TEM. Addition of Li^+ and Na^+ did not lead to the formation of aggregates. A more indirect measurement of aggregation by diffusion NMR (DOSY) supported the electron microscope results. Most interestingly, in the presence of Cs^+ the reaction is both the fastest and ~fourth order in Mn(IV)-OH-PFOM. This supports a mechanistic hypothesis that a 4 Mn(IV)-OH centered complex is viable and a possible reactive state for O_2 formation. Notably, this observation was made possible because in such an *intermolecular assembly* the Mn−Mn distances are much longer than known for the oxygen evolving complex of PSII. The slower reaction enabled the study of the reactivity of an isolated species. It would appear that a bimolecular mechanism for O_2 formation is also feasible but significantly slower.

EXPERIMENTAL SECTION

Synthesis. *$K_{16}[NaH_2Mn(II)W_{17}F_6O_{55}]_2{\cdot}40H_2O$, Mn(II)PFOM.* The Mn(II) substituted polyfluoroxometalate, Mn(II)PFOM, was synthesized by a previously reported method.[13] First the Zn(II) substituted polyfluoroxometalate is prepared by dissolving 44 g of $Na_2WO_4{\cdot}2H_2O$ in 100 mL of deionized water and heating to 80−85 °C. To this solution are added about 14 mL of 40% HF bringing it to pH = 4.5. The solution is then stirred for 1 h and filtered. The filtrate is then reheated to 80 °C and a solution of 7 g $Zn(CH_3CO_2)_2{\cdot}2H_2O$ in 10 mL of deionized water is added dropwise. The solution is let to stir for an additional 1 h and then filtered. Note that carefully controlling the temperature insures that the zinc atom is substituted at the belt position only. This filtrate is precipitated by addition of 4.5 g KCl and the precipitate is recrystallized in 5.5 mL deionized water. Yield 3 g. See the Supporting Information for further analysis of Zn(II)PFOM. Then 3 g of Zn(II)PFOM dissolved in 27 mL of acetate buffer, pH = 5, is heated to 50 °C and 324 mg $MnSO_4{\cdot}H_2O$ in 2 mL of acetate buffer, pH = 5, are added dropwise. The solution turns brown, is stirred for 30 min and then cooled and precipitated with a saturated solution of KCl. Yield 2.4 g (80%). Elemental analysis Calcd (Exp): Na, 0.47 (0.35); K, 7.16 (6.46); Mn, 1.12 (0.76); W, 63.63 (62.67); H_2O (TGA), 5.64 (7.34). IR 724, 776, 813, 882, 949 cm^{-1}. Crystallization yielded mostly a dimer, which is in equilibrium with the monomer as explained above. See Table 3 for details on the dimer.

$K_8[NaH_2Mn(III)(H_2O)W_{17}F_6O_{55}]{\cdot}13H_2O$, Mn(III)PFOM. Mn(II)-PFOM, 200 mg, were dissolved in 6 mL of deionized water and 114 mg of $K_2S_2O_8$ were added. The solution was heated until the purple color started turning brown. Mn(III)PFOM was crystallized in the presence of ethanol vapor that serves both as a reducing agent and an antisolvent. After a few days purple crystals of $Mn^{(III)}$PFOM were formed. Yield 180 mg (90%). Elemental analysis Calcd (Exp): Na, 0.47 (0.37); K, 6.42 (6.18); Mn, 1.13 (0.87); W, 64.14 (64.73); H_2O (TGA), 6.77 (4.94). IR 737, 786, 888, 954 cm^{-1}.

$K_8[NaH_2Mn(IV)(OH)W_{17}F_6O_{55}]{\cdot}15H_2O$, Mn(IV)PFOM. Method 1: 2 g of Mn(II)PFOM were dissolved in 10 mL of double distilled water and treated with a flow of 6.2 mg ozone per min for 30 min. The color of the solution changed to dark brown and Mn(IV)PFOM is collected from a frozen solution by lyophilization. Yield 1.7 g (85%). *Method 2*: 2 g of Mn(II)PFOM were dissolved in 35 mL of deionized water; 2 g of Oxone was added and the solution was heated to 80 °C. The

DOI: 10.1021/jacs.5b03456
J. Am. Chem. Soc. 2015, 137, 8738−8748

solution changed color from light brown to purple and finally to dark brown, whereupon it is cooled in ice water and Mn(IV)PFOM is collected by precipitation with saturated KCl. X-ray quality crystals were grown at 4 °C. Yield 1.2 g (60%). Elemental analysis Calcd (Exp): Na, 0.47 (0.35); K, 6.42 (6.40); Mn, 1.13 (0.72); W, 64.16 (65.71); H_2O (TGA), 6.45 (5.63). IR 731, 784, 836, 890, 954 cm^{-1}.

$K_7[NaH_2Mn(V)(OH)W_{17}F_6O_{55}]\cdot 20H_2O$, Mn(V)PFOM. Two grams of Mn(II)PFOM were dissolved in 65 mL of double distilled water and placed into a pressure tube. 1.6 g of $K_2S_2O_8$ were added. The pressure tube was sealed and heated in an oil-bath at 160 °C. A color change from light brown to purple to dark brown and finally to green was observed. After 30 min the pressure tube was cooled and a small amount of fine brown precipitate that was formed is removed by centrifugation. The filtrate was then reduced to 30 mL by evaporation, and Mn(V)PFOM was precipitated with a saturated KCl solution. Finally the product is recrystallized in 1 mL of deionized water at 80 °C. Yield 0.9 g (57%). Elemental analysis Calcd (Exp): Na, 0.47 (0.35); K, 5.66 (5.46); Mn, 1.13 (0.84); W, 64.67 (63.99); H_2O (TGA), 5.23 (7.43). IR 739, 778, 886, 955 cm^{-1}.

X-ray Crystallography. Data were collected and processed either by a Nonius KappaCCD diffractometer or a Bruker Appex2 KappaCCD diffractometer; Mo Kα (λ = 0.71073 Å), graphite monochromator. The data were processed with Denzo-scalepack, and the structures were solved by direct methods with SHELXS. The data are summarized in Table 3.

Magnetic Susceptibility. Magnetic susceptibility was measured at RT using a Guoy magnetic balance. The diamagnetic correction was made by measuring the magnetic susceptibility of the structurally similar Zn(II)PFOM. Magnetic susceptibility was also measured during cooling and heating of the samples at $2 \leq T \leq 300$ K and H = 5000 Oe by SQUID magnetometer (MPMS3). The diamagnetic correction was made by fitting Mn(II)PFOM assuming no TIP and applying the same correction to all other oxidation states.

X-ray Photoelectron Spectroscopy (XPS). XPS measurements were conducted on a Kratos Axis-Ultra DLD with a monochromatized Al source operated at 15 W. Detection at pass energies ranging between 20 and 80 eV was used, whereas most of our line-shape analysis was based on data recorded at pass energy = 40 eV. Charge compensation was attempted by means of a flood gun, used at 1.8 Å and 0.5 V filament bias, while the charge balance was set to 0.5 V. The X-ray source was with a pass energy of 40 eV. Data collected for W $4f^{7/2}$, W $4f^{5/2}$ and W $5p^{3/2}$ was baseline corrected with a Shirley-type background and fitted with a function consisting of a series of 3 Gaussian equations adapted in advance for the specific line shape of these peaks. Mn $2p^{3/2}$ and Mn $2p^{1/2}$ peaks were treated in a similar way. See the Supporting Information for the equations used. Finally, the binding energies of W $4f^{7/2}$ were subtracted from those of Mn $2p^{3/2}$ in order to correct for the differential charging effects, assuming that the W $4f^{7/2}$ binding energy is negligibly modified only for the different oxidation states of manganese.

X-ray Absorption Spectroscopy (XAS). Samples for the XAS experiments were prepared by diluting the MnPFOM solid with solid boron nitride in a mass ratio of 1:6. The mixture was thoroughly ground for 30 min and a uniform thin layer of the sample was brushed onto a piece of tape, which was then folded to ensure a homogeneous powder distribution. XAS data were collected at beamline X3B at the National Synchrotron Light Source (NSLS) of Brookhaven National Laboratory. Mn K-edge XAS data were collected for frozen solutions maintained at ~20 K over the energy range 6.3−7.4 keV. A Mn foil spectrum was measured simultaneously for internal energy calibration using the first inflection point of the K-edge energy (6539.0 eV). Data were obtained as fluorescence excitation spectra using a solid-state germanium detector (Canberra). Data reduction, averaging, and normalization were performed using the program EXAFSPAK.[29] The coordination number of a given shell was a fixed parameter and was varied iteratively in integer steps while the bond lengths (R) and mean-square deviation (σ^2) were allowed to freely float. The amplitude reduction factor was fixed at 0.9 while the edge-shift parameter E_0 was allowed to float as a single value for all shells. The pre-edge features were fit using the Fityk program[30] with pseudo-Voigt functions composed of 50:50 Gaussian/Lorentzian functions (Figure S8).

Electron Microscopy (STEM and TEM). Samples for electron microscopy were prepared from solutions of 4.5 mM Mn(IV)-OH-PFOM and 70 mM of MCl (M = Li, Na, K, Rb or Cs) at 60 °C. A drop of solution was put on a Quantifoil grid kept at high humidity and maintained at 60 °C in the chamber of the automated plunging apparatus (Leica EM-GP). The grid was then blotted with filter paper and plunged into liquid ethane. Samples were transferred under liquid nitrogen to a Gatan 626 cryoholder, and visualized by TEM and STEM under low-dose cryo-conditions with a Tecnai G2 TWIN-F20 microscope. TEM images were recorded on a Gatan US4000 CCD camera, and STEM images were recorded with a Fischione HAADF detector.

Diffusion Ordered Spectroscopy (DOSY). Samples were prepared from solutions of 4.5 mM Zn(II)PFOM and 70 mM MCl (M = Li, Na, K, Rb or Cs) in D_2O. The measurements were performed on a Bruker 400 MHz NMR using the dstebpgp3s pulse sequence provided by Bruker at 353.2K. The parameters used were: diffusion period Δ = 0.2s and the gradient pulse length δ = 7.5 ms. 32 different exponentially distributed gradient strengths were measured. The results were analyzed by the CONTIN method provided in the TopSpin program.

Quantification of O_2 Evolution. 0.4 mL of 46 mM Mn(IV)-OH-PFOM in double distilled water were inserted into a 2 mL vial and sealed with a septum. The vial was then purged with CO_2 for 10 min in order to remove all air. 120 μL of N_2O were inserted to the vial as an internal standard. The vial was left overnight at 70 °C to react. Finally, the amount of O_2 in the gas phase of the vial was quantified by gas chromatography by integrating the peak area of O_2 versus that of N_2O. The gas chromatograph instrument that was used was a HP-6890 equipped with a microthermal conductivity detector and a ShinCarbon ST 80/100 Micropacked Column 2m × 0.53 mm ID and a 250 μL injection port valve. Helium was used as carrier gas. Retention times O_2 1.1 min; CO_2 7.9 min; N_2O 9.4 min.

■ ASSOCIATED CONTENT

Supporting Information

Additional NMR, XPS, XAS, kinetic, X-ray diffraction and magnetic susceptibility data. The Supporting Information is available free of charge on the ACS Publications website at DOI: 10.1021/jacs.5b03456.

■ AUTHOR INFORMATION

Corresponding Author

*ronny.neumann@weizmann.ac.il

Notes

The authors declare no competing financial interest.

■ ACKNOWLEDGMENTS

This research at the Weizmann Institute was supported by the Israel Science Foundation Grant #763/14, the I-CORE Program of the Planning and Budgeting Committee and The Israel Science Foundation (Grant 152/11), the Helen and Martin Kimmel Center for Molecular Design. Electron microscopy was performed at the Irving and Cherna Moscowitz Center for Nano and Bio-Nano Imaging of the Weizmann Institute of Science. R.N. is the Rebecca and Israel Sieff Professor of Chemistry. The work carried out at the University of Minnesota was supported by the U.S. National Science Foundation (CHE-1361773 to L.Q.). XAS data were collected on beamline X3B at the National Synchrotron Radiation Lightsource (NSLS), which is supported by the U.S. Department of Energy under Contract No. DE-AC02-98CH10886. Use of beamline X3B was made possible by the Center for

DOI: 10.1021/jacs.5b03456
J. Am. Chem. Soc. 2015, 137, 8738−8748

Synchrotron Biosciences Grant, P30-EB-00998, from the National Institute of Biomedical Imaging and Bioengineering.

REFERENCES

(1) (a) Whittaker, J. W. *Arch. Biochem. Biophys.* **2012**, *525*, 111−120. (b) Wu, A. J.; Penner-Hahn, J. E.; Pecoraro, V. L. *Chem. Rev.* **2004**, *104*, 903−938.

(2) (a) Sheng, Y.; Abreu, I. A.; Cabelli, D. E.; Maroney, M. J.; Miller, A.-F.; Teixeira, M.; Valentine, J. S. *Chem. Rev.* **2014**, *114*, 3854−3918. (b) Riley, D. P. *Chem. Rev.* **1999**, *99*, 2573−2587.

(3) (a) Yano, J.; Yachandra, V. *Chem. Rev.* **2014**, *114*, 4175−4205. (b) Wiechen, M.; Najafpour, M. M.; Allakhverdiev, S. I.; Spiccia, L. *Energy Environ. Sci.* **2014**, *7*, 2203−2212. (c) Tsui, E. Y.; Kanady, J. S.; Agapie, T. *Inorg. Chem.* **2013**, *52*, 13833−13848.

(4) (a) Hage, R.; de Boer, J. W.; Gaulard, F.; Maaijen, K. *Adv. Inorg. Chem.* **2013**, *65*, 85−116. (b) Saisaha, P.; de Boer, J. W.; Browne, W. R. *Chem. Soc. Rev.* **2013**, *42*, 2059−2074. (c) Costas, M. *Coord. Chem. Rev.* **2011**, *255*, 2912−2932.

(5) (a) Groves, J. T.; Kruper, W. J., Jr.; Haushalter, R. C. *J. Am. Chem. Soc.* **1980**, *102*, 6375−6377. (b) Groves, J. T.; Stern, M. K. *J. Am. Chem. Soc.* **1988**, *110*, 8628−8638. (c) Jin, N.; Ibrahim, M.; Spiro, T. G.; Groves, J. T. *J. Am. Chem. Soc.* **2007**, *129*, 12416−12417. (d) Song, W. J.; Seo, M. S.; DeBeer George, S.; Ohta, T.; Song, R.; Kang, M.-J.; Tosha, T.; Kitagawa, T.; Solomon, E. I.; Nam, W. *J. Am. Chem. Soc.* **2007**, *129*, 1268−1277. (e) Zhang, R.; Newcomb, M. *Acc. Chem. Res.* **2008**, *41*, 468−477. (f) Baglia, R. A.; Durr, M.; Ivanovic-Burmazovic, I.; Goldberg, D. P. *Inorg. Chem.* **2014**, *53*, 5893−5895. (g) Guo, M.; Dong, H.; Li, J.; Cheng, B.; Huang, Y.-Q.; Feng, Y.-Q.; Lei, A. *Nat. Commun.* **2012**, *3*, 2196/1−2196/9. (h) Fukuzumi, S.; Mizuno, T.; Ojiri, T. *Chem.—Eur. J.* **2012**, *18*, 15794−15804. (i) Crestoni, M. E.; Fornarini, S.; Lanucara, F. *Chem.—Eur. J.* **2009**, *15*, 7863−7866. (j) Lee, J. Y.; Lee, Y.-M.; Kotani, H.; Nam, W.; Fukuzumi, S. *Chem. Commun.* **2009**, 704−706.

(6) (a) Liu, H.-Y.; Mahmood, M. H. R.; Qiu, S.-X.; Chang, C. K. *Coord. Chem. Rev.* **2013**, *257*, 1306−1333. (b) Abu-Omar, M. M. *Dalton Trans.* **2011**, *40*, 3435−3444. (c) Gross, Z. *J. Biol. Inorg. Chem.* **2001**, *6*, 733−738. (d) Kumar, A.; Goldberg, I.; Botoshansky, M.; Buchman, Y.; Gross, Z. *J. Am. Chem. Soc.* **2010**, *132*, 15233−15245. (e) Kim, S. H.; Park, H.; Seo, M. S.; Kubo, M.; Ogura, T.; Klajn, J.; Gryko, D. T.; Valentine, J. S.; Nam, W. *J. Am. Chem. Soc.* **2010**, *132*, 14030−14032. (f) Liu, H.-Y.; Fei, Y.; Xie, Y.-T.; Li, X.-Y.; Chang, C. K. *J. Am. Chem. Soc.* **2009**, *131*, 12890−12891.

(7) (a) Neu, H. M.; Yang, T.; Baglia, R. A.; Yosca, T. H.; Green, M. T.; Quesne, M. G.; de Visser, S. P.; Goldberg, D. P. *J. Am. Chem. Soc.* **2014**, *136*, 13845−13852. (b) Jung, J.; Ohkubo, K.; Prokop-Prigge, K. A.; Neu, H. M.; Goldberg, D. P.; Fukuzumi, S. *Inorg. Chem.* **2013**, *52*, 13594−13604. (c) Prokop, K. A.; Goldberg, D. P. *J. Am. Chem. Soc.* **2012**, *134*, 8014−8017. (d) Prokop, K. A.; Neu, H. M.; de Visser, S. P.; Goldberg, D. P. *J. Am. Chem. Soc.* **2011**, *133*, 15874−15877. (e) Fukuzumi, S.; Kotani, H.; Prokop, K. A.; Goldberg, D. P. *J. Am. Chem. Soc.* **2011**, *133*, 1859−1869. (f) Lansky, D. E.; Goldberg, D. P. *Inorg. Chem.* **2006**, *45*, 5119−5125. (g) Lansky, D. E.; Mandimutsira, B.; Ramdhanie, B.; Clausen, M.; Penner-Hahn, J.; Zvyagin, S. A.; Telser, J.; Krzystek, J.; Zhan, R.; Ou, Z.; Kadish, K. M.; Zakharov, L.; Rheingold, A. L.; Goldberg, D. P. *Inorg. Chem.* **2005**, *44*, 4485−4498.

(8) (a) Taguchi, T.; Gupta, R.; Lassalle-Kaiser, B.; Boyce, D. W.; Yachandra, V. K.; Tolman, W. B.; Yano, J.; Hendrich, M. P.; Borovik, A. S. *J. Am. Chem. Soc.* **2012**, *134*, 1996−1999. (b) MacDonnell, F. M.; Fackler, N. L. P.; Stern, C.; O'Halloran, T. V. *J. Am. Chem. Soc.* **1994**, *116*, 7431. (c) Yatabe, T.; Kikunaga, T.; Matsumoto, T.; Nakai, H.; Yoon, K.-S.; Ogo, S. *Chem. Lett.* **2014**, *43*, 1380−1382. (d) Koikawa, M.; Okawa, H.; Kida, S. *J. Chem. Soc., Dalton Trans.* **1988**, 641−645. (e) Garcia-Bosch, I.; Company, A.; Cady, C. W.; Styring, S.; Browne, W. R.; Ribas, X.; Costas, M. *Angew. Chem., Int. Ed.* **2011**, *50*, 5648−5653. (f) Collins, T. J.; Powell, R. D.; Slebodnick, C.; Uffelmann, E. S. *J. Am. Chem. Soc.* **1990**, *112*, 899−901. (g) Collins, T. J.; Gordonwlie, S. W. *J. Am. Chem. Soc.* **1989**, *111*, 4511−4513. (h) Workman, J. M.; Powell, R. D.; Procyk, A. D.; Collins, T. J.; Bocian, D. F. *Inorg. Chem.* **1992**, *31*, 1548−1550. (i) Chattopadhyay, S.; Geiger, R. A.; Yin, G.; Busch, D. H.; Jackson, T. A. *Inorg. Chem.* **2010**, *49*, 7530−7535. (j) Taguchi, T.; Stone, K. L.; Gupta, R.; Kaiser-Lassalle, B.; Yano, J.; Hendrich, M. P.; Borovik, A. S. *Chem. Sci.* **2014**, *5*, 3064−3071. (k) Yin, G. *Acc. Chem. Res.* **2013**, *46*, 483−492.

(9) (a) Al-Oweini, R.; Sartorel, A.; Bassil, B. S.; Natali, M.; Berardi, S.; Scandola, F.; Kortz, U.; Bonchio, M. *Angew. Chem., Int. Ed.* **2014**, *53*, 11182−11185. (b) Yin, Q.; Tan, J. M.; Besson, C.; Geletii, Y. V.; Musaev, D. G.; Kuznetsov, A. E.; Luo, Z.; Hardcastle, K. I.; Hill, C. L. *Science* **2010**, *328*, 342−345. (c) Huang, Z.; Luo, Z.; Geletii, Y. V.; Vickers, J. W.; Yin, Q.; Wu, D.; Hou, Y.; Ding, Y.; Song, J.; Musaev, D. G.; Lian, T.; Hill, C. L. *J. Am. Chem. Soc.* **2011**, *133*, 2068−2071. (d) Goberna-Ferron, S.; Vigara, L.; Soriano-Lopez, J.; Galan-Mascaros, J. R. *Inorg. Chem.* **2012**, *51*, 11707−11715. (e) Tanaka, S.; Annaka, M.; Sakai, K. *Chem. Commun.* **2012**, *48*, 1653−1655. (f) Wu, J.; Liao, L.; Yan, W.; Xue, Y.; Sun, Y.; Yan, X.; Chen, Y.; Xie, Y. *ChemSusChem* **2012**, *5*, 1207−1212. (g) Stracke, J. J.; Finke, R. G. *J. Am. Chem. Soc.* **2011**, *133*, 14872−14875. (h) Natali, M.; Berardi, S.; Sartorel, A.; Bonchio, M.; Campagna, S.; Scandola, F. *Chem. Commun.* **2012**, *48*, 8808−8810. (i) Lieb, D.; Zahl, A.; Wilson, E. F.; Streb, C.; Nye, L. C.; Meyer, K.; Ivanovic-Burmazovic, I. *Inorg. Chem.* **2011**, *50*, 9053−9058. (j) Lv, H.; Song, J.; Geletii, Y. V.; Vickers, J. W.; Sumliner, J. M.; Musaev, D. G.; Kögerler, P.; Zhuk, P.; Bacsa, J.; Zhu, G.; Hill, C. L. *J. Am. Chem. Soc.* **2014**, *136*, 9268−9271. (k) Vickers, J. W.; Lv, H.; Sumliner, J. M.; Zhu, G.; Luo, Z.; Musaev, D. G.; Geletii, Y. V.; Hill, C. L. *J. Am. Chem. Soc.* **2013**, *135*, 14110−14118.

(10) (a) Hill, C. L.; Brown, R. B. *J. Am. Chem. Soc.* **1986**, *108*, 536−537. (b) Mansuy, D.; Bartoli, J. F.; Battioni, P.; Lyon, D. K.; Finke, R. G. *J. Am. Chem. Soc.* **1991**, *113*, 7222−7229. (c) Neumann, R.; Khenkin, A. M. *Chem. Commun.* **1998**, 1967−1968. (d) Neumann, R.; Gara, M. *J. Am. Chem. Soc.* **1994**, *116*, 5509−5510. (e) Neumann, R.; Gara, M. *J. Am. Chem. Soc.* **1995**, *117*, 5066−5074. (f) Neumann, R.; Juwiler, D. *Tetrahedron* **1996**, *47*, 8781−8788. (g) Boesing, M.; Noeh, A.; Loose, I.; Krebs, B. *J. Am. Chem. Soc.* **1998**, *120*, 7252−7259. (h) Ben-Daniel, R.; Weiner, L.; Neumann, R. *J. Am. Chem. Soc.* **2002**, *124*, 8788−8789.

(11) Khenkin, A. M.; Kumar, D.; Shaik, S.; Neumann, R. *J. Am. Chem. Soc.* **2006**, *128*, 15451−15460.

(12) Barats-Damatov, D.; Shimon, L. J. W.; Weiner, L.; Schreiber, R. E.; Jiménez-Lozano, P.; Poblet, J. M.; de Graaf, C.; Neumann, R. *Inorg. Chem.* **2014**, *53*, 1779−1787.

(13) Ben-Daniel, R.; Khenkin, A. M.; Neumann, R. *Chem.—Eur. J.* **2000**, *6*, 3722−3728.

(14) Khenkin, A. M.; Neumann, R. *Inorg. Chem.* **2000**, *39*, 3455−3462.

(15) This study, which is not directly related to the topic of this research will be published separately.

(16) Ressler, T.; Wong, J.; Roos, J.; Smith, I. L. *Environ. Sci. Technol.* **2000**, *34*, 950−958.

(17) Westre, T. E.; Kennepohl, P.; Dewitt, J. G.; Hedman, B.; Hodgson, K. O.; Solomon, E. *J. Am. Chem. Soc.* **1997**, *119*, 6297−6314.

(18) (a) Yachandra, V. K.; Guiles, R. D.; McDermott, A.; Britt, R. D.; Dexheimer, S. L.; Sauer, K.; Klein, M. P. *Biochim. Biophys. Acta, Bioenerg.* **1986**, *850*, 324−332. (b) Leto, D. F.; Jackson, T. A. *Inorg. Chem.* **2014**, *53*, 6179−6194.

(19) Tourné, C. M.; Tourné, G. F.; Zonnevijlle, F. *J. Chem. Soc., Dalton Trans.* **1991**, 143−155å.

(20) Gupta, R.; MacBeth, C. E.; Young, V. G.; Borovik, A. S. *J. Am. Chem. Soc.* **2002**, *124*, 1136−1137.

(21) (a) Collins, T. J.; Gordon-Wylie, S. W. *J. Am. Chem. Soc.* **1989**, *111*, 4511−4513. (b) Collins, T. J.; Powell, R. D.; Slebodnick, C.; Uffelman, E. S. *J. Am. Chem. Soc.* **1990**, *112*, 899−901. (c) MacDonnell, F. M.; Fackler, N. L.; Stern, C.; O'Halloran, T. V. *J. Am. Chem. Soc.* **1994**, *116*, 7431−7432.

(22) The magnetic susceptibility behavior at low temperatures indicates a possibility of Mn−F interactions, which leads to deviation from the Curie law at low temperatures.

DOI: 10.1021/jacs.5b03456
J. Am. Chem. Soc. 2015, 137, 8738−8748

(23) Note that the actual oxidation potentials could not be measured by CV because they are higher than the oxidation potentials of water, see Figure S19.
(24) Spitsyn, V. I.; Babaev, N. B. *Russ. J. Inorg. Chem.* **1960**, *å*, 580−585.
(25) In solution the polyoxometalate-based colloids are in dynamic equilibrium and not static. The time scale of a dynamic light scattering (DLS) measurement is such that unreliable results were obtained.
(26) It is our supposition that the lower rates observed upon addition of K^+ and Rb^+ are related to the degree of aggregation and/or a combination of a four- and two- manganese centered reaction pathways.
(27) Kok, B.; Forbush, B.; McGloin, M. *Photochem. Photobiol.* **1970**, *11*, 467−475.
(28) (a) Krewald, V.; Retegan, M.; Cox, N.; Messinger, J.; Lubitz, W.; DeBeer, S.; Neese, F.; Pantazis, D. A. *Chem. Sci.* **2015**, *6*, 1676−1695. (b) Cox, N.; Retegan, M.; Neese, F.; Pantazis, D. A.; Boussac, A.; Lubitz, W. *Science* **2014**, *345*, 804−808.
(29) George, G. N. *EXAFSPAK*; Stanford Synchrotron Radiation Laboratory: Stanford, CA, 1990.
(30) Fityk: a general-purpose peak fitting program. Wojdyr, M. *J. Appl. Crystallogr.* **2010**, *43*, 1126−1128.

DOI: 10.1021/jacs.5b03456
J. Am. Chem. Soc. 2015, 137, 8738−8748